Blind Source Separation of Color Noisy Blurred Images

Giulio Biondi, Antonio Boccuto, and Ivan Gerace(✉)

Department of Mathematics and Computer Science, University of Perugia, Perugia, Italy
{giulio.biondi,antonio.boccuto,ivan.gerace}@unipg.it

Abstract. Blind Source Separation (BSS) is a relevant problem in the signal processing research area, with a broad application sphere. In this work, we consider a BSS problem with recto–verso images subject to show–through and bleed–through effects; in particular, we suppose that the observed image is obtained using a two-step linear process: the recto and verso images are separately blurred using a blur operator with known coefficients and then mixed. Our algorithm, Blind Estimation Technique Imposing Smoothness and Non–Overlapping (BETIS–NO), built on top of previous work, computes the entries of the mixture matrix, which regulates the intensity of recto–verso mixing for the document reconstruction; the introduction of second–order discontinuities and additional constraints on source images, i.e., minimum entropy, non–Gaussianity, and correct overlapping, leads to improved quality of the reconstruction.

Keywords: Blind Source Separation · Regularization · Indirect Maximum A Priori estimation · Graduate Non–Convex algorithm

1 Introduction

This paper deals with the Blind Source Separation (BSS) problem, a popular topic within the broader research area of signal processing. The BSS problem consists of separating source signals from a group of mixed signals without knowing the mixing coefficients and is relevant to several research fields, e.g., separating individual speech signals from mixed audio signals in the cocktail party problem [2], classifying images, detecting changes in images, identifying the structure of buildings in thermographic images for seismic engineering [9], and estimating the Cosmic Microwave Background (CMB) from galactic and extragalactic emissions (see, e.g., [12,20]).

In this work, we focus on digitally restoring degraded written documents, which can suffer damage from various sources such as weathering, ink seepage, humidity, powder, mold, and light transmission. Over time, these factors can cause paper and ink to deteriorate, leading to the degradation and decay of written records. In particular, we address two types of effects in degraded written documents: show–through and bleed–through. Show–through is caused by the

© The Author(s), under exclusive license to Springer Nature Switzerland AG 2023
O. Gervasi et al. (Eds.): ICCSA 2023 Workshops, LNCS 14108, pp. 659–675, 2023.
https://doi.org/10.1007/978-3-031-37117-2_44

transparency of the paper, resulting in the text from one side appearing on the other due to the light used in the scanning process. Conversely, bleed–through is caused by ink seeping through the paper, producing a similar effect to show–through. The physical model for show-through distortion is complex, considering factors such as paper features, transmittance parameters, the reflectance of the verso, and how light spreads through the paper.

Removing the bleed–through (or the show–through) patterns from a digital document scan is generally challenging, especially in ancient documents, where the interferences are often significant. Indeed, dealing with heavy bleed-through using a simple threshold technique is practically ineffective since the intensities of the unwanted ink filtered from the back can be similar to those of the main text. For instance, in [21], several threshold techniques are compared for separating text in degraded historical documents; in general, both global and local thresholds do not provide satisfactory results.

In this work, we assume that the decayed image is formed through a two-step linear process: the recto and verso images are separately blurred using a blur operator with known coefficients and then mixed [8,13,28]. The mixture matrix defines the mixing intensity and will be subject to estimation during the document reconstruction phase. The problem is said to be non–blind when the mixture matrix is known; both the blind and the non–blind problems are ill–posed (see also [16]). Regularization techniques can convert an ill–posed non–blind BSS problem into a well–posed one by addressing the instability problem. Such techniques require solving a nearby well–posed problem with specific known properties, which has a unique stable solution. Piecewise smoothness is often assumed for the estimated sources, and the solution to the inverse problem is determined by minimizing an appropriate energy function.

To solve the blind BSS problem of estimating the mixture matrix, we use a target function. We start by considering a mixture matrix and computing the related sources by minimizing the energy function. Then, we evaluate the properties of the result using the target function, defined as a combination of various terms that represent constraints based on our prior knowledge about the solution. Using this function, we can determine the effectiveness of the estimated solution in meeting our restrictions and producing the desired results. This technique is called *Indirect Maximum A Priori* (IMAP) estimation (see, e.g., [8,10,12,13,15]).

In particular, in this article, differing from how it was done in [8], where the *Blind Estimation Technique Imposing Smoothness* (BETIS) technique was proposed, we impose that the ideal sources are piecewise linear, do not present adjacent parallel discontinuities (see also [3,5,6]), and are non–Gaussian (see also [18,19]). Additionally, we impose that the values of the front and back are partially overlapping, classifying our method as a *Correlated Component Analysis* (CCA) technique [1,4]. Furthermore, we introduce a new measure of the system entropy and use it in the target function.

A stochastic algorithm such as *Simulated Annealing* (SA) minimizes the target function. During the target function minimization, it is necessary tominimize

the energy function, which is generally non-convex; for this purpose, we apply a *Graduate Non-Convexity* (GNC)-algorithm (see, e.g., [3,6,7,11,17,22–25,27,29]). We refer to our technique as *Blind Estimation Technique Imposing Smoothness and Non–Overlapping* (BETIS–NO).

The paper is structured as follows. In Sect. 2, we describe the background mathematical model; in Sect. 3, we first deal with the non–blind reconstruction, using regularization techniques; in Sect. 4, we deal with the blind problem using an IMAP approach; in Sect. 5, we show the effectiveness of our algorithm using the presented experimental results.

2 Mathematical Model

We begin with defining the *source recto-verso document* as a vector $\mathbf{s} \in \mathbb{R}^{6MN}$, where M and N are the dimensions of the recto and the verso of the analyzed document, structured as follows:

$$\mathbf{s} = \left((\mathbf{s}_f^{(r)})^T \ (\mathbf{s}_f^{(g)})^T \ (\mathbf{s}_f^{(b)})^T \ (\mathbf{s}_v^{(r)})^T \ (\mathbf{s}_v^{(g)})^T \ (\mathbf{s}_v^{(b)})^T \right)^T, \tag{1}$$

where each block of the vector $\mathbf{s}$ in (Eq. 1) is an $M \times N$-dimensional vector, taken in the lexicographic order. Hereafter, the index f (resp., v) corresponds to the front (resp., verso), while the symbols (r), (g), (b) are associated with the colors red, green, and blue, respectively.

We assume that the blur operator acting on the visible (resp., hidden) side of the image is given by

$$H_k = \begin{pmatrix} H_k^{(r,r)} & H_k^{(r,g)} & H_k^{(r,b)} \\ H_k^{(g,r)} & H_k^{(g,g)} & H_k^{(g,b)} \\ H_k^{(b,r)} & H_k^{(b,g)} & H_k^{(b,b)} \end{pmatrix},$$

where $k = 1$ (resp., $k = 2$). The $H_k^{(u,v)}$'s, $u, v \in \{r, g, b\}$, $k = 1, 2$, can be easily derived from a given blur mask $M_k^{(u,v)} \in \mathbb{R}^{(2\rho+1)\times(2\rho+1)}$, whose radius is denoted by ρ (see, e.g., [6,14]). We assume that the observed document is obtained using the following model:

$$\mathbf{m} = \begin{pmatrix} \mathbf{m}_f^{(r)} \\ \mathbf{m}_f^{(g)} \\ \mathbf{m}_f^{(b)} \\ \mathbf{m}_v^{(r)} \\ \mathbf{m}_v^{(g)} \\ \mathbf{m}_v^{(b)} \end{pmatrix} = \begin{pmatrix} a_{1,1}H_1 & a_{1,2}H_2 \\ a_{2,1}H_1 & a_{2,2}H_2 \end{pmatrix} \begin{pmatrix} \mathbf{s}_f^{(r)} \\ \mathbf{s}_f^{(g)} \\ \mathbf{s}_f^{(b)} \\ \mathbf{s}_v^{(r)} \\ \mathbf{s}_v^{(g)} \\ \mathbf{s}_v^{(b)} \end{pmatrix} + \mathbf{n} = \mathcal{H}(A)\mathbf{s} + \mathbf{n}, \tag{2}$$

where

$$A = \begin{pmatrix} a_{1,1} & a_{1,2} \\ a_{2,1} & a_{2,2} \end{pmatrix}$$

is the mixture matrix, which describes how the observed images are obtained from the ideal source images, and the vector $\mathbf{n}$, of dimension MN, is the additive noise, which we assume to be white, Gaussian, with zero mean and a known variance σ^2.

The linear *Blind Source Separation* (BSS) problem consists in reconstructing the original source $\mathbf{s}$ and to evaluate the matrix A, starting from the mixture vector $\mathbf{m}$. Here we assume that the linear operators $H_k^{(u,v)}$, $u, v \in \{r, g, b\}$, $k = 1, 2$, and the variance of the noise are known.

3 Non-blind Reconstruction

Let us consider first the non–blind problem, in which the mixture matrix A is known. This problem is ill–posed in the sense of Hadamard (see, e.g., [16]). To regularize the problem, we now introduce the second–order finite difference operators. Note that it has been proved experimentally that the use of such operators yields better results than that of operators of first or third order (see, e.g., [7]). A *clique* c of order 2 is a subset of points of a square grid on which the second–order finite difference is defined. We denote by the symbol C_2 the set of all cliques of order 2, namely $C_2 = \{c = \{(i,j),(h,l),(r,q)\} : i = h = r, j = l+1 = q+2 \text{ or } i = h+1 = r+2, j = l = q\}$. Every element of C_2 is uniquely associated with a discontinuity of order 2, which is labeled with a hidden line element.

We denote the second order finite difference operator of the vector $\mathbf{s}_k^{(e)}$, $e \in \{r, g, b\}$, $k = 1, 2$, associated with the clique c, by $D_c^2 \mathbf{s}_k^{(e)}$, that is, if $c = \{(i,j),(h,l),(r,q)\} \in C_2$, then $D_c^2 \mathbf{s}_k^{(e)} = s_k^{(e)}(i,j) - 2s_k^{(e)}(h,l) + s_k^{(e)}(r,q)$. Let us introduce the concept of *adjacent clique of order* 2, used to define the non-parallelism constraint, whose importance is apparent in Fig. 1. The original image in (a) is blurred to obtain (b); (c) is reconstructed from (b) without imposing the non-parallelism constraint, while the image in (d) is obtained by enforcing it. The reconstructions of Figure Fig. 1(c) and (d) present significant differences in terms of artifacts, which are also evident in the corresponding line process plots (e) and (f). Note that this example is given in the simplified case where only the reconstruction of a blurred image is required.

Given a vertical clique $c = \{(i,j),(i+1,j),(i+2,j)\}$, $i = 3, \ldots, M-2$, $j = 1, \ldots, N$, we define its preceding clique $c-1$ as follows:

$$c - 1 = \{(i-2,j),(i-1,j),(i,j)\}.$$

If c is a horizontal clique, $c = \{(i,j),(i,j+1),(i,j+2)\}$, $i = 1, \ldots, M$, $j = 3, \ldots, N-2$, then its preceding clique $c-1$ is defined by setting

$$c - 1 = \{(i,j-2),(i,j-1),(i,j)\}.$$

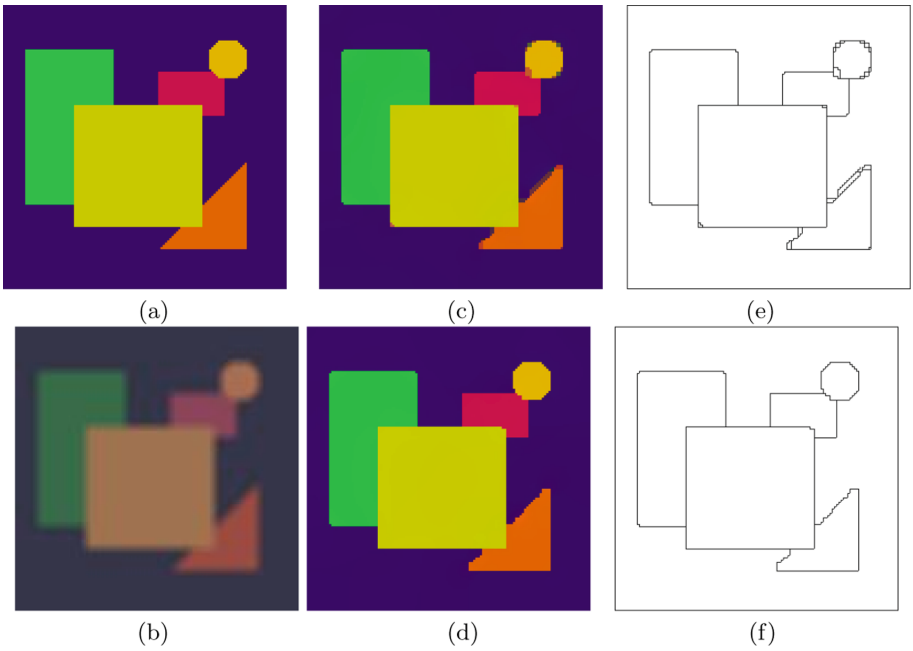

Fig. 1. The original (resp., blurred) image is in (a) (resp., (b)); the image reconstructed without (resp., with) non-parallelism constraint is given in (c) (resp., (d)), with line elements drawn in (e) (resp., (f)).

Given a mixture matrix A, We define a *regularized solution* $\widetilde{\mathbf{s}}$ as an argument of the minimum of the energy function defined by

$$E_A(\mathbf{s}) = \|\mathbf{m} - \mathcal{H}(A)\mathbf{s}\|_2^2 + \sum_{k=1}^{2} \sum_{c \in C_2} \varphi(N_c^2 \mathbf{s}_k, N_{c-1}^2 \mathbf{s}_k) + \sum_{k=1}^{2} \sum_{c \in C_2} \varphi(V_c^2 \mathbf{s}_k, V_{c-1}^k \mathbf{s}_k), \tag{3}$$

where $\|\cdot\|_2$ is the Euclidean norm, and the first term of the right hand of (Eq. 3) indicated a data faithfulness constraint. The second term in the right hand of (Eq. 3) expresses the intra–channel smoothness of the images. The third term indicates a correlation between the different channels, i.e., an inter–channel smoothness. Intra–channel and inter–channel smoothness are measured using the operators N_c^2 and V_c^2, respectively, and φ is a stabilizer associated with the requested degree of smoothness and which relaxes it when one expects a discontinuity (see, e.g., [5,6]).

We begin with defining the operator N_c^2, i.e. the norm of the vector of the finite differences of the intensities of the red, green, and blue channels evaluated

on the clique c of second order, as follows:

$$N_c^2 \mathbf{s}_k = \left\| \left(D_c^2 \mathbf{s}_k^{(r)}, D_c^2 \mathbf{s}_k^{(g)}, D_c^2 \mathbf{s}_k^{(b)} \right) \right\|_2, \ k = 1, 2, \tag{4}$$

where $\mathbf{s}_k = ((\mathbf{s}_k^{(r)})^T, (\mathbf{s}_k^{(g)})^T, (\mathbf{s}_k^{(b)})^T)^T$, and D_c^2 is a finite difference operator of order 2 applied to a suitable set c of adjacent pixels, as defined above.

The inter-channel correlation is strictly related to the clue of the objects in the image; for this reason, the finite difference operators should enforce the same coherent behavior for all the channels. Thus we define the following operators:

$$V_c^2 \mathbf{s}_k = \left\| \left(D_c^2 \mathbf{s}_k^{(r)} - D_c^2 \mathbf{s}_k^{(g)}, D_c^2 \mathbf{s}_k^{(r)} - D_c^2 \mathbf{s}_k^{(b)}, D_c^2 \mathbf{s}_k^{(g)} - D_c^2 \mathbf{s}_k^{(b)} \right) \right\|_2, \ k = 1, 2, \tag{5}$$

which are the norms of the vector of the inter-channel differences of the intra-channel derivatives of the second order.

In (Eq. 3), N_c^2 and V_c^2 are weighted by suitable stabilizers, which should regulate the requested degree of smoothness and relax it when discontinuities are expected.

To have a more precise reconstruction, it is fundamental that discontinuities are not thick; that is, the object contours are not blurred. So, it is advisable to avoid discontinuities at two adjacent cliques. In particular, to prevent double discontinuities, we deal with a function φ, bivariate concerning the operators defined in (Eq. 4) and (Eq. 5) in the cliques c and $c-1$, respectively. When $c-1$ is not defined, we assume directly that the adjacent discontinuity is null.

Thus, we use a two-variable function $\varphi : \mathbb{R} \times \mathbb{R} \to \mathbb{R}$ (see also [6]), defined by

$$\varphi(t_1, t_2) = \begin{cases} g_1(t_1), & \text{if } |t_2| \le s, \\ \left(1 - \frac{2(|t_2|-s)^2}{(\zeta-s)^2}\right) g_1(t_1) + \frac{2(|t_2|-s)^2}{(\zeta-s)^2}\, g_2(t_1), & \text{if } s < |t_2| \le \frac{\zeta+s}{2}, \\ \frac{2(|t_2|-\zeta)^2}{(\zeta-s)^2}\, g_1(t_1) + \left(1 - \frac{2(|t_2|-\zeta)^2}{(\zeta-s)^2}\right) g_2(t_1), & \text{if } \frac{\zeta+s}{2} < |t_2| < \zeta, \\ g_2(t_1), & \text{if } |t_2| \ge \zeta, \end{cases} \tag{6}$$

where

$$s = \frac{\sqrt{\alpha}}{\lambda},$$

and ζ is such that $\zeta - s$ is a positive and sufficiently small quantity, and for $i = 1, 2$ we have

$$g_i(t_1) = \begin{cases} \lambda^2 t_1^2, & \text{if } |t_1| < q_i, \\ \alpha_i - \dfrac{\tau}{2}(|t_1| - r_i)^2, & \text{if } q_i \le |t_1| \le r_i, \\ \alpha_i, & \text{if } |t_1| > r_i, \end{cases}$$

$$\alpha_i = \begin{cases} \alpha, & \text{if } i = 1, \\ \alpha + \varepsilon, & \text{if } i = 2, \end{cases} \qquad q_i = \frac{\sqrt{\alpha_i}}{\lambda^2} \left(\frac{2}{\tau} + \frac{1}{\lambda^2} \right)^{-1/2},$$

τ is a large enough real constant, and

$$r_i = \frac{\alpha_i}{\lambda^2 q_i}, \quad i = 1, 2.$$

The graph of the function in (Eq. 6) for some values of the parameters is pictured in Fig. 2(a).

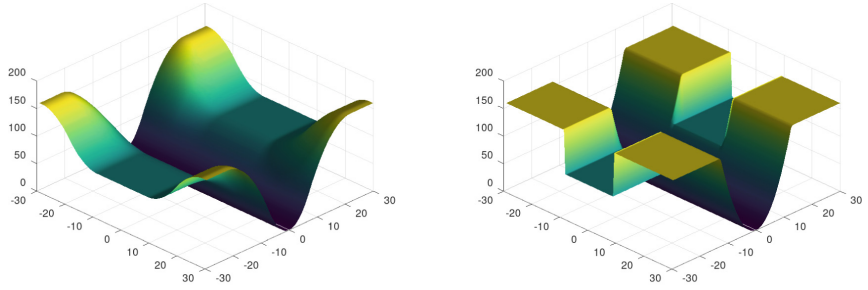

(a) (b)

Fig. 2. Used stabilizers with $\lambda = 1$, $\alpha = \varepsilon = 80$.

Observe that, when $\zeta - s = 0$ and τ tends to $+\infty$, we get an ideal model with Boolean line variables (see Fig. 2(b)), where λ^2 is a regularization parameter, which regulates the smoothness of the solution, α is the cost to introduce a discontinuity on the image. Such a cost is incremented by ε if there is a parallel discontinuity. In [5] a duality-type theorem was proved, which states that the use of a suitable bivariate function, as the one defined in (Eq. 6), preserves the edges in the reconstructed images and prevents parallel edges from appearing. Additionally, in (Eq. 6) the underlying line elements assume a continuous range of values.

4 IMAP Estimation

Now we deal with the blind problem. In this context, both the sources and the mixture matrix are unknown. The estimate of the mixture matrix is defined as

$$\widetilde{A} = \arg\min_{A} F(A, \mathbf{s}(A)),$$

where F is the *target function*, that is constructed in order to find the solution which best fits the a priori knowledge, and

$$\mathbf{s}(A) = \arg\min_{\mathbf{s}} E_A(\mathbf{s}).$$

The solution to the blind problem is given by $(\tilde{\mathbf{s}} = \mathbf{s}(\tilde{A}), \tilde{A})$. Such a technique is called *Indirect Maximum A Priori* (IMAP) (see, e.g., [8,10,12,13,15]). In this paper, we propose the following target function:

$$\begin{aligned} F(\mathbf{s}(A)) = \omega_1\, NG(\mathbf{s}(A)) + \omega_2\, OV(\mathbf{s}(A)) + \omega_3\, EN(\mathbf{s}(A)) \\ + \sum_{k=1}^{2} \sum_{c \in C_2} \varphi(N_c^2 \mathbf{s}_k, N_{c-1}^2 \mathbf{s}_k) + \sum_{k=1}^{2} \sum_{c \in C_2} \varphi(V_c^2 \mathbf{s}_k, V_{c-1}^k \mathbf{s}_k), \end{aligned} \tag{7}$$

where $NG(\mathbf{s}(A))$ measures the non–Gaussianity of the estimated source $\mathbf{s}(A)$, $OV(\mathbf{s}(A))$ expresses the overlapping degree of $\mathbf{s}_1(A)$ over $\mathbf{s}_2(A)$, $EN(\mathbf{s}(A))$ denotes the entropy of the estimated source $\mathbf{s}(A)$ and the last two terms measure to which extent the constructed sources are suitably smooth and without double edges, concerning both inter-channel and intra-channel components. The parameters ω_i, $i = 1, 2, 3$, express the strength of the imposed constraints.

To minimize the target function $F(\mathbf{s}(A))$ in (Eq. 7), a stochastic algorithm such as *Simulated Annealing* (SA) is used. During the target function minimization, it is necessary to minimize the energy function $E(\mathbf{s})$ in (Eq. 3). Note that $E(\mathbf{s})$ is in general non-convex. So, we apply a *Graduate Non-Convexity* (GNC)-technique in order to minimize $E(\mathbf{s})$ (see, e.g., [3,6,7,11,17,22–25,27,29]). Hereafter, we refer to the proposed technique as BETIS–NO (*Blind Estimation Technique Imposing Smoothness and Non-Overlapping*), while we name its previous version proposed in [8] as BETIS (*Blind Estimation Technique Imposing Smoothness*).

4.1 The Non–Gaussianity Constraint

To measure the Gaussianity of a grayscale image $\mathbf{y} \in \mathbb{R}^{NM}$, we first find the histogram of $\mathbf{y}$, by defining the following function:

$$d_{\mathbf{y}}(\eta) = \#(\{y_{i,j} : y_{i,j} = \eta,\, i = 1, \ldots, M,\, j = 1, \ldots, N\}), \quad \eta = 0, 1, \ldots, 255,$$

where $\#(\cdot)$ denotes the cardinality of a generic set; in the color case, three histograms can be computed, one for each color component. Now, we denote by $\Phi_{\mu,\sigma}$ the Gaussian function with mean μ and standard deviation σ, and define the distance of a histogram of an image $\mathbf{y}$ from a Gaussian curve of mean μ and variance σ by setting

$$G(\mathbf{y}, \mu, \sigma) = \sum_{\eta=0}^{255} (d_{\mathbf{y}}(\eta) - \Phi_{\mu,\sigma}(\eta))^2. \tag{8}$$

Given a fixed image $\mathbf{y}$, we deal with finding that values of μ and σ which minimize the function G defined in (Eq. 8). This function is not convex in (μ, σ). So, we estimate a suitable componentwise minimum. Starting with the mean

μ and the standard deviation σ of the histogram $d(\mathbf{y})$, we apply the following heuristic (where h is a suitable small enough step):

```
change=true;
while change
        change=false;
        while G(y, μ, σ) > G(y, μ − h, σ)
                μ = μ − h;
                change=true;
        end while
        while G(y, μ, σ) > G(y, μ + h, σ)
                μ = μ + h;
                change=true;
        end while
        while G(y, μ, σ) > G(y, μ, σ − h)
                σ = σ − h;
                change=true;
        end while
        while G(y, μ, σ) > G(y, μ, σ + h)
                σ = σ + h;
                change=true;
        end while
end while
```

We define as $\mu(\mathbf{y})$ and $\sigma(\mathbf{y})$ those expressions obtained in the above heuristic. Thus, we define the *non–Gaussianity* of the estimated source $\mathbf{s}$ by

$$NG(\mathbf{s}) = \sum_{\mathbf{k=1}}^{\mathbf{2}} \sum_{\mathbf{e}\in\{\mathbf{r},\mathbf{g},\mathbf{b}\}} \frac{\mathbf{1}}{\mathbf{G}(\mathbf{s_k^{(e)}}, \mu(\mathbf{s_k^{(e)}}), \sigma(\mathbf{s_k^{(e)}}))}.$$

4.2 Overlapping Constraint

In a document, there is an overlapping when a value different from the background of the recto overlaps with an analogous element of the verso. To correctly separate two images, it is advisable to estimate the overlapping level present in the ideal sources. A technique to determine such a level was given in [4] in the case of non–blurred and non–noisy images, and a related quick algorithm was presented. Thus, to reduce computational costs, we use such an estimate by calling it $RO(\mathbf{s})$. We define our error concerning a correct overlapping level as

$$OV(\mathbf{s}) = \left(RO(\mathbf{s}) - \sum_{e\in\{r,g,b\}} \sum_{i=1}^{N} \sum_{j=1}^{M} \left((\overline{m}_1^{(e)} - s_1^{(e)}(i,j))(\overline{m}_2^{(e)} - s_1^{(e)}(i,j) \right)^2 \right)^2$$

where $\overline{m}_k^{(e)}$, $k = 1, 2$, is the median of the image $\mathbf{s}_k^{(e)}$. We assume that such medians correspond with the background of the involved images.

4.3 Entropy Constraint

To measure the entropy, it is necessary to compute the number of states ι of the studied system; in our case ι expresses the gray levels present in an image $\mathbf{y}$, i.e.

$$\iota(\mathbf{y}) = \#(\{\eta \in \{0, \ldots, 255\} : d_{\mathbf{y}}(\eta) \neq 0\}).$$

In Fig. 3(a) and (c), the two possible ideal sources are shown, while in (e) mixture of the ideal images after separately blurring them and adding noise. Please note that the blurring level is generally different between the front and the verso; moreover, the cardinality of the set of states is directly correlated to the sharpness of an image: sharper images have fewer states, as visible in Fig. 3(b), (d), and (e).

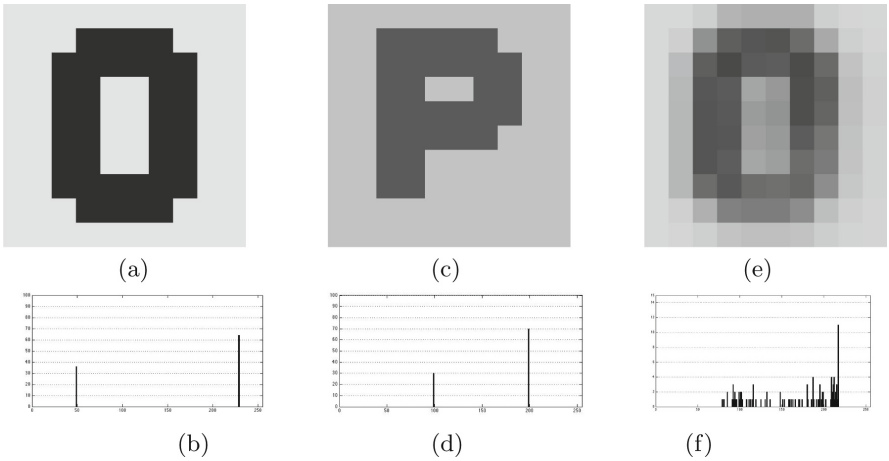

Fig. 3. In (a) and (c), there are the front and the verso of the ideal document, respectively; a mixture of such sources is given in (e). In (b), (d), and (f), there are the corresponding histograms.

Thus, we define the *entropy level* of the estimated source $\mathbf{s}$ as

$$EN(\mathbf{s}) = k_B \ \ln\left(\sum_{k=1}^{2}\sum_{e\in\{r,g,b\}} \iota(\mathbf{s}_k^{(e)})\right),$$

where k_B is the Boltzmann constant.

5 Experimental Results

The presented experimental results are divided into two parts. In the former, we show a quantitative comparison between BETIS presented in [8] and the here proposed BETIS–NO. For this purpose, synthetic data are generated through the linear model given in (Eq. 2) and then reconstructed; the quality of reconstructions is measured by the MSE (mean square error) between the real and the reconstructed sources. Note that other algorithms in the literature are not directly comparable because of the difference in the data generation model. We also chose to replicate the same experimental results given in [8] to evaluate the BETIS algorithm to provide a better comparison with it. Later, we evaluate qualitatively our algorithm in the reconstruction of real data mixtures.

The following blur masks are used to generate synthetic data from ideal images:

$$M_1^{(u,u)} = \begin{pmatrix} 0\,1\,2\,1\,0 \\ 1\,2\,4\,2\,1 \\ 2\,4\,9\,4\,2 \\ 1\,2\,4\,2\,1 \\ 0\,1\,2\,1\,0 \end{pmatrix}, \quad M_2^{(u,u)} = \begin{pmatrix} 0\,1\,2\,1\,0 \\ 1\,2\,2\,2\,1 \\ 2\,2\,6\,2\,2 \\ 1\,2\,2\,2\,1 \\ 0\,1\,2\,1\,0 \end{pmatrix},$$

for $u \in \{r, g, b\}$, while $M_k^{(u,v)} = \frac{1}{3} M_k^{(u,u)}$ for $u, v \in \{r, g, b\}$, $u \neq v$, $k = 1, 2$. A Gaussian noise is added, with the characteristics in Sect. 2, and standard deviation $\sigma = 5$. The parameters used in the reconstruction are always $\lambda = 0.5$, $\alpha = 10$, $\epsilon = 10$, $\omega_1 = 5 \cdot 10^5$, $\omega_2 = 0.5$, and $\omega_3 = 1 \cdot 10^4$.

Here we assume that the sum of all the rows of the mixture matrix is equal to one, since we expect the background color of the source to be the same as that of the data (see [4]).

In Fig. 4, in (a) and (b) the front and retro ideal images are shown; in (c) and (d) the generated mixtures are present; in (e) and (f) we see the sources estimated by BETIS, while in (g) and (h) there are those estimated by BETIS–NO.

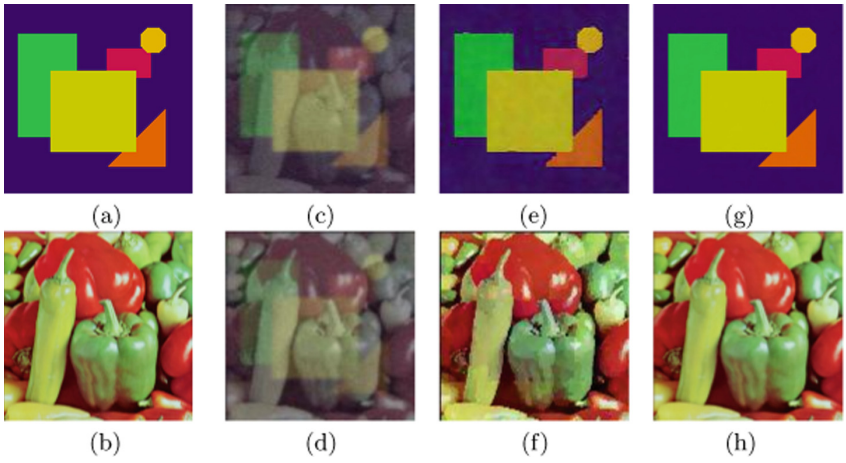

Fig. 4. (a) and (b): ideal images; (c) and (d): generated mixtures; (e) and (f): sources estimated by BETIS; (g) and (h): sources estimated by BETIS–NO.

In Fig. 5 and Fig. 6 we show, in the same order as in Fig. 4, the respective documents and the related reconstructions.

In Table 1 the mixture matrices used to generate the synthetic data and those obtained in BETIS and BETIS–NO are shown. In Table 2 we present the mean square errors between the ideal sources and those estimated by BETIS and BETIS–NO. It is apparent that the reconstruction computed by BETIS–NO is significantly closer to the original than that of BETIS, due to the introduction of the new proposed constraints.



Fig. 5. (a) and (b): ideal images; (c) and (d): generated mixtures; (e) and (f): sources estimated by BETIS; (g) and (h): sources estimated by BETIS–NO.

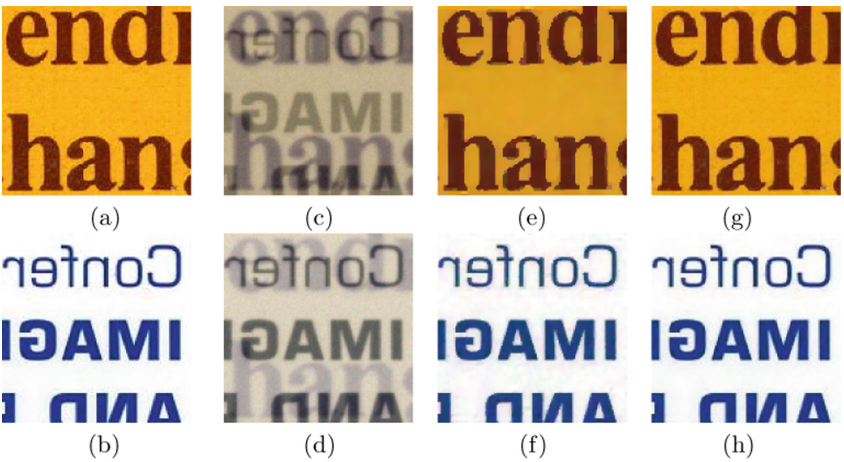

Fig. 6. (a) and (b): ideal images; (c) and (d): generated mixtures; (e) and (f): sources estimated by BETIS; (g) and (h): sources estimated by BETIS–NO.

Table 1. Original and estimated mixture matrices

Experiment	Real mixture matrix	Mixture matrix obtained by BETIS	Mixture matrix obtained by BETIS–NO
1	$\begin{pmatrix} 0.7124 & 0.2876 \\ 0.4281 & 0.5719 \end{pmatrix}$	$\begin{pmatrix} 0.7489 & 0.2511 \\ 0.4784 & 0.5216 \end{pmatrix}$	$\begin{pmatrix} 0.7165 & 0.2835 \\ 0.4305 & 0.5695 \end{pmatrix}$
2	$\begin{pmatrix} 0.7023 & 0.2977 \\ 0.3812 & 0.6188 \end{pmatrix}$	$\begin{pmatrix} 0.7367 & 0.2633 \\ 0.3925 & 0.6075 \end{pmatrix}$	$\begin{pmatrix} 0.7038 & 0.2962 \\ 0.3841 & 0.6159 \end{pmatrix}$
3	$\begin{pmatrix} 0.7103 & 0.2897 \\ 0.3086 & 0.6914 \end{pmatrix}$	$\begin{pmatrix} 0.7023 & 0.2977 \\ 0.3112 & 0.6888 \end{pmatrix}$	$\begin{pmatrix} 0.7105 & 0.2895 \\ 0.3074 & 0.6926 \end{pmatrix}$

Table 2. MSE of the algorithms BETIS and BETIS–NO

Experiment	BETIS		BETIS–NO	
	MSE recto	MSE verso	MSE recto	MSE verso
1	430.8025	604.8162	6.6897	11.4097
2	357.5233	192.1110	54.9735	26.0081
3	574.7180	186.4750	87.3849	22.8117

Now we present some results obtained starting from the real mixtures. In Fig. 7, we show the reconstructions using BETIS and BETIS–NO of a document affected by the show–through effect. No blur operator was considered in this case. It is visibly evident that the result obtained by BETIS–NO improves that given by BETIS.

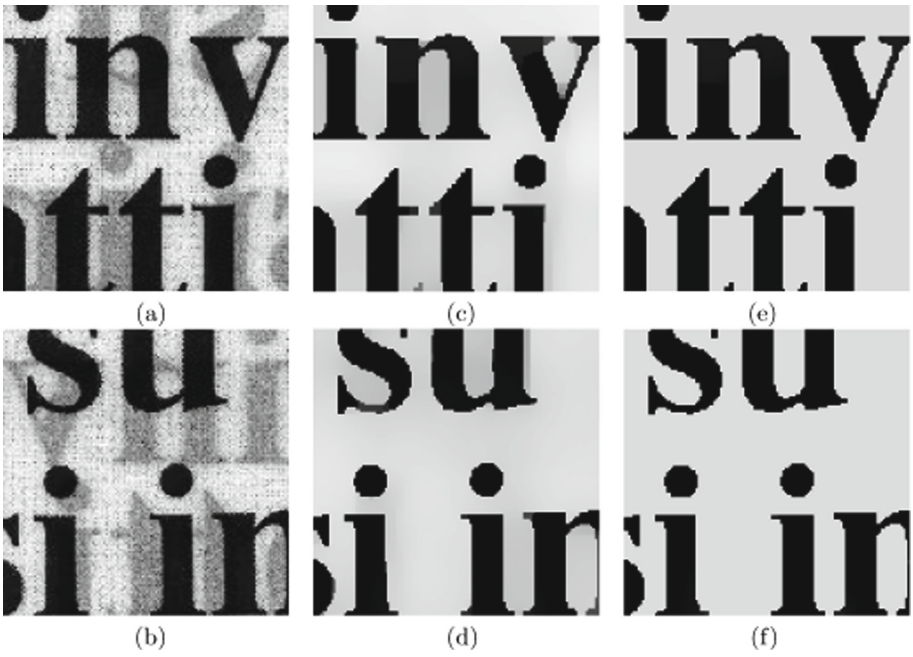

Fig. 7. (a) and (b): real mixtures; (c) and (d): sources estimated by BETIS; (e) and (f): sources estimated by BETIS–NO.

The data document in Fig. 8 (a) and (b) is taken from the database created as part of the *Irish Script on Screen* (ISOS) project of the School of Celtic Studies of the Dublin Institute for Advanced Studies, in conjunction with the SIGMEDIA group of the Department of Electrical and Electronic Engineering

at Trinity College Dublin (see [26]). This database contains ancient documents affected by bleed–through. Here, we empirically assumed that the blur masks are as follows.

$$M_1^{(u,u)} = \begin{pmatrix} 0 & 0 & O \\ 0 & 1 & 0 \\ 0 & 0 & 0 \end{pmatrix}, \quad M_2^{(u,u)} = \begin{pmatrix} 0 & 1 & O \\ 1 & 4 & 1 \\ 0 & 1 & 0 \end{pmatrix},$$

for $u \in \{r, g, b\}$, while $M_k^{(u,v)} = \frac{1}{6} M_k^{(u,u)}$ for $u, v \in \{r, g, b\}$, $u \neq v$, $k = 1, 2$. In Fig. 8(c) and (d) the reconstruction obtained by BETIS–NO is presented.

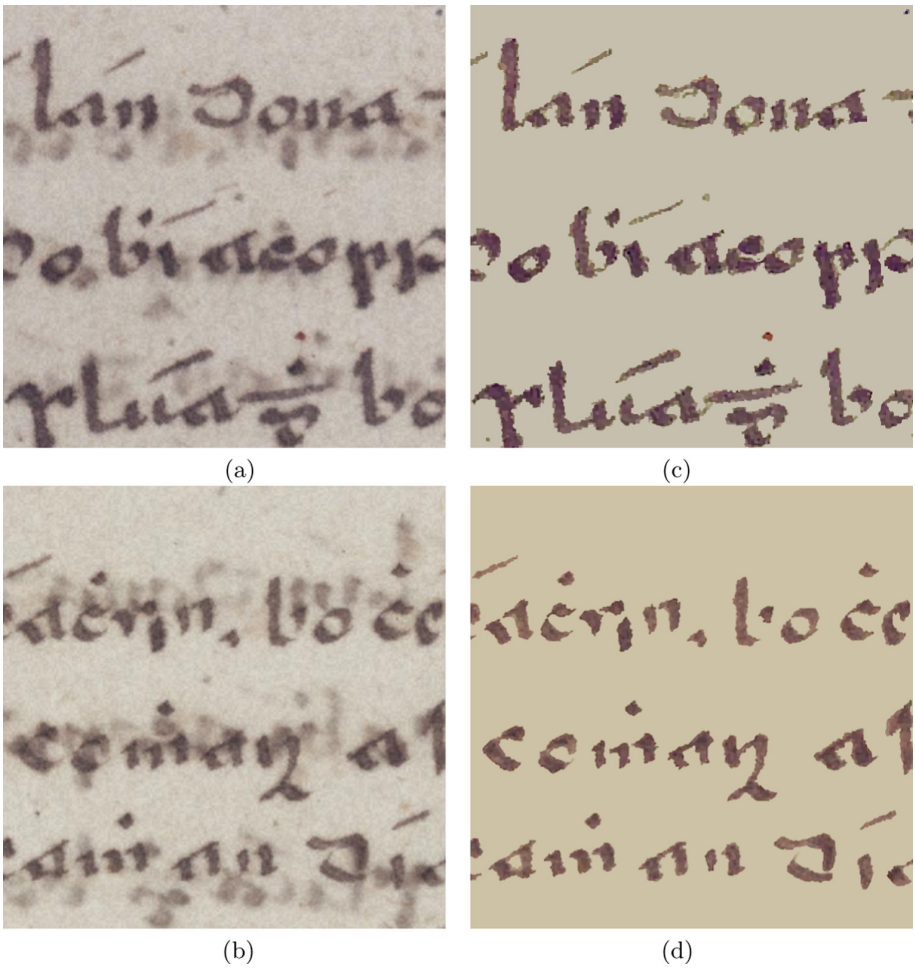

Fig. 8. (a) and (b): real mixtures; (c) and (d): sources estimated by BETIS–NO.

Conclusions

In this work, we dealt with a BSS problem in which we assumed that the decayed image is formed through a two-step linear process: the recto and verso images are separately blurred using a blur operator with known coefficients and then mixed. Our algorithm estimates the entries of the mixture matrix, which controls the intensity of recto-verso mixing for the document reconstruction. Our IMAP-type approach, BETIS–NO, is built on top of previous work [8] and enhanced by introducing second–order discontinuities and additional constraints on source images, i.e., minimum entropy, non–Gaussianity, and correct overlapping. The experimental results show the promising capability of the algorithm in reconstructing original documents, measured for synthetic data through MSE, and analyzed through visual inspection for real data. We could further extend the proposed technique by incorporating the blur mask's estimation into the mixture matrix's estimation; however, by increasing the degrees of freedom in our field of research, a significant increase in computational cost must be expected.

References

1. Barros, A.K.: The independence assumption: dependent component analysis. In: Girolami, M. (eds.) Advances in Independent Component Analysis. Perspectives in Neural Computing. Springer, London (2000). https://doi.org/10.1007/978-1-4471-0443-8_4
2. Benlin, X., Fangfang, L., Xingliang, M., Huazhong, J.: Study on independent component analysis application in classification and change detection of multispectral images. In: The International Archives of the Photogrammetry, Remote Sensing, and Spatial Information Sciences, vol. 37, pp. 871–876 (2008)
3. Boccuto, A., Gerace, I.: Image reconstruction with a non-parallelism constraint. In: Proceedings of the International Workshop on Computational Intelligence for Multimedia Understanding, Reggio Calabria, Italy, 27–28 October 2016, pp. 1–5. IEEE Conference Publications (2016)
4. Boccuto, A., Gerace, I., Giorgetti, V.: A blind source separation technique for document restoration. SIAM J. Imaging Sci. **12**(2), 1135–1162 (2019)
5. Boccuto, A., Gerace, I., Martinelli, F.: Half-quadratic image restoration with a non-parallelism constraint. J. Math. Imaging Vis. **59**(2), 270–295 (2017)
6. Boccuto, A., Gerace, I., Pucci, P.: Convex approximation technique for interacting line elements deblurring: a new approach. J. Math. Imaging Vis. **44**(2), 168–184 (2012)
7. Cricco, F., De Santi, G., Gerace, I.: A deterministic algorithm for deblurring considering higher order smoothness constraints. In: Proceedings of the 2003 International Workshop on Spectral Methods and Multirate Signal Processing SMMSP2004, Vienna, Austria, 11/12 September 2004, pp. 325–332 (2004)
8. Cricco, F., Gerace, I.: An IMAP estimation for the joint separation and restoration of mixed degraded color images. In: Proceedings of the 7th Conference on Applied and Industrial Mathematics in Italy, Venice (Italy), 20–24 September 2004, pp. 260–269 (2004)
9. Cluni, F., Costarelli, D., Minotti, A.M., Vinti, G.: Applications of sampling Kantorovich operators to thermographic images for seismic engineering. J. Comput. Anal. Appl. **19**(4), 602–617 (2015)

10. Discepoli, M., Gerace, I., Pandolfi, R.: Blind image restoration from multiple views by IMAP estimation. In: Modern Information Processing From Theory to Applications, pp. 441–452 (2006)
11. Evangelopoulos, X., Brockmeier, A. J., Mu, T., Goulermas, J. Y.: A graduated non-convexity relaxation for large-scale seriation. In: Proceedings of the 2017 SIAM International Conference on Data Mining, Houston, Texas (USA), pp. 462–470 (2017)
12. Fedeli, L., Gerace, I., Martinelli, F.: Unsupervised blind separation and deblurring of mixtures of sources. In: Proceedings of Knowledge-Based Intelligent Information and Engineering Systems. LNCS, Vietri sul Mare, Italy, vol. 4694, pp. 25–32 (2007)
13. Gerace, I., Cricco, F., Tonazzini, A.: An extended maximum likelihood approach for the robust blind separation of autocorrelated images from noisy mixtures. In: Puntonet, C.G., Prieto, A. (eds.) ICA 2004. LNCS, vol. 3195, pp. 954–961. Springer, Heidelberg (2004). https://doi.org/10.1007/978-3-540-30110-3_120
14. Gerace, I., Pandolfi, R.: A color image restoration with adjacent parallel lines inhibition. In: Proceedings of the 12th International Conference on Image Analysis and Processing, 17–19 September 2003, Mantova, Italy, 6 p. (2003)
15. Gerace, I., Pandolfi, R., Pucci, P.: A new estimation of blur in the blind restoration problem. In: Proceedings of the 2003 International Conference on Image Processing, Barcelona, Spain, 14–17 September 2003, pp. 261–264 (2003)
16. Gillis, N.: Sparse and unique nonnegative matrix factorization through data preprocessing. J. Mach. Learn. Res. **13**, 3349–3386 (2012)
17. Hazan, E., Levy, K.Y., Shalev-Shwartz, S.: On graduated optimization for stochastic non-convex problems. In: Proceedings of the 33rd International Conference on Machine Learning, New York, NY, USA, vol. 48, pp. 1–9, 2016. JMLR: W& CP (2016)
18. Hyvärinen, A.: Fast and robust fixed-point algorithms for independent component analysis. IEEE Trans. Neural Netw. **10**, 626–634 (1999)
19. Hyvärinen, A.: Gaussian moments for noisy independent component analysis. IEEE Sig. Proc. Lett. **6**, 145–147 (1999)
20. Kuruoglu, E., Bedini, L., Paratore, M.T., Salerno, E., Tonazzini, A.: Source separation in astrophysical maps using independent factor analysis. Neural Netw. **16**(3–4), 479–491 (2003)
21. Leedham, G., Varma, S., Patankar, A., Govindaraju, V.: Separating text and background in degraded document images - a comparison of global thresholding techniques for multi-stage thresholding. In: Proceedings of the 8th International Workshop on Frontiers in Handwriting Recognition, Niagara on the Lake, Canada, pp. 244–249 (2002)
22. Liu, Z.-Y., Qiao, H.: GNCCP-graduated nonconvexity and concavity procedure. IEEE Trans. Pattern Anal. Mach. Intell. **36**(6), 1258–1267 (2014)
23. Liu, Z.-Y., Qiao, H., Su, J.-H.: MAP inference with MRF by graduated non-convexity and concavity procedure. In: Loo, C.K., Yap, K.S., Wong, K.W., Teoh, A., Huang, K. (eds.) ICONIP 2014. LNCS, vol. 8835, pp. 404–412. Springer, Cham (2014). https://doi.org/10.1007/978-3-319-12640-1_49
24. Nikolova, M., Ng, M.K., Tam, C.-P.: On ℓ_1 data fitting and concave regularization for image recovery. SIAM J. Sci. Comput. **35**(1), A397–A430 (2013)
25. Nikolova, M., Ng, M.K., Zhang, S., Ching, W.-K.: Efficient reconstruction of piecewise constant images using nonsmooth nonconvex minimization. SIAM J. Imaging Sci. **1**(1), 2–25 (2008)

26. Rowley-Brooke, R., Pitié, F., Kokaram, A.: A ground truth bleed-through document image database. In: Zaphiris, P., Buchanan, G., Rasmussen, E., Loizides, F. (eds.) TPDL 2012. LNCS, vol. 7489, pp. 185–196. Springer, Heidelberg (2012). https://doi.org/10.1007/978-3-642-33290-6_21
27. Smith, T., Egeland, O.: Dynamical pose estimation with graduated non-convexity for outlier robustness. Model. Identif. Control (MIC) J. **43**(2), 79–89 (2022)
28. Tonazzini, A., Gerace, I., Martinelli, F.: Document image restoration and analysis as separation of mixtures of patterns: from linear to nonlinear models. In: Gunturk, B.K., Li, X. (eds.) Image Restoration - Fundamentals and Advances, pp. 285–310. CRC Press, Taylor & Francis, Boca Raton (2013)
29. Yang, H., Antonante, P., Tzoumas, V., Carlone, L.: Graduated non-convexity for robust spatial perception: from non-minimal solvers to global outlier rejection. IEEE Robot. Autom. Lett. **5**(2), 1127–1134 (2020)